Article

Characterization of Solid-State Dye-Sensitized Solar Cells Utilizing High Absorption Coefficient Metal-Free Organic Dyes

Wendy H. Howie, Frederik Claeyssens, Hidetoshi Miura, and Laurence M. Peter

J. Am. Chem. Soc., **2008**, 130 (4), 1367-1375 • DOI: 10.1021/ja076525+

J|A|C|S
ARTICLES
Published on Web 01/05/2008

Characterization of Solid-State Dye-Sensitized Solar Cells Utilizing High Absorption Coefficient Metal-Free Organic Dyes

Wendy H. Howie,[†] Frederik Claeyssens,[‡] Hidetoshi Miura,[§] and Laurence M. Peter*,[†]

Department of Chemistry, University of Bath, Bath BA2 7AY, United Kingdom, School of Chemistry, University of Bristol, Bristol BS8 1TS, United Kingdom, and Chemicrea Inc., Tsukuba Centre, 2-1-6 Sengen, Tsukuba, Ibaraki 305-0047, Japan

Received August 29, 2007; E-mail: l.m.peter@bath.ac.uk

Abstract: Solid-state dye-sensitized solar cells were fabricated using the organic hole-transporting medium (HTM) 2,2′7,7′-tetrakis-(*N*,*N*-di-*p*-methoxyphenyl-amine)-9,9′-spirobifluorene (spiro-MeOTAD), and three organic indoline-based sensitizer dyes with high molar extinction coefficients. The cells were characterized by several techniques, including spectral response measurements, photovoltage decay transients, intensity modulated photovoltage spectroscopy (IMVS), and charge extraction. The differences in apparent electron lifetime observed for cells fabricated using the three dyes are attributed in part to changes in the surface dipole potential at the TiO_2/spiro-MeOTAD interface, which shift the TiO_2 conduction band energy relative to the Fermi level of the HTM. These energy shifts influence both the open circuit voltage (as a result of changes in free electron density) and the short circuit current (as a consequence of changes in the overlap between the dye LUMO level and the conduction band). A self-consistent approach was used to derive the positions of the conduction band relative to the spiro-MeOTAD redox Fermi level for cells fabricated using the three dyes. The analysis also provided estimates of the free electron lifetime in spiro-MeOTAD cells. In order to evaluate the possible contribution of the adsorbed dyes to the observed changes in surface dipole potential, their dipole moments were estimated using ab initio density functional theory (DFT) calculations. Comparison of the calculated dipole contributions with the experimentally measured shifts in conduction band energy revealed that other factors such as proton adsorption may be predominant in determining the surface dipole potential.

Introduction

AM 1.5 power conversion efficiencies exceeding 11% have been reported for dye-sensitized solar cells (DSC),[1] suggesting that they have the potential to compete with other thin film photovoltaic devices. In a DSC, light absorbed by a monolayer of dye molecules chemisorbed on a porous layer of nanocrystalline metal oxide (usually TiO_2) results in rapid electron injection into the conduction band of the oxide. The injected electrons move through the interconnected mesoporous metal oxide network by trap-limited diffusion (random walk) and are extracted at the transparent conducting glass anode. The porous oxide layer is permeated with a redox electrolyte (I_3^-/I^-), which regenerates the dye in its original oxidation state via electron transfer. The oxidized component of the redox system (I_3^-) diffuses to the platinized cathode, where it is reduced to I^- to complete the regenerative cycle.

Conventional DSCs use a ruthenium bipyridyl sensitizer dye such as bis(tetrabutylammonium) *cis*-bis(thiocyanato)bis(2,2′-bypiridine-4,4′-dicarboxylato)ruthenium(II)[2,3] (N719: ϵ =14,000 M^{-1} cm^{-1} at 541 nm) with a volatile nonaqueous I^-/I_3^- electrolyte. An alternative to the liquid electrolyte is a solid, organic, hole-transporting material (HTM) such as spiro-MeOTAD (2,2′7,7′-tetrakis-(*N*,*N*-di-*p*-methoxyphenyl-amine)-9,9′-spirobifluorene).[4−6] The redox potential for spiro-MeOTAD is reported to be 0.55V vs Ag/AgCl,[7] which is 0.45 V more positive than the redox potential of the I/I_3^-[8] couple in the organic solvents used in a DSC, so that, in principle at least, spiro-MeOTAD cells should give higher open circuit voltages.

Since current methods for fabricating spiro-MeOTAD-based DSCs can result in poor pore filling of the organic hole conductor in the mesoporous layer, thin TiO_2 films (1.5−3 μm)

[†] University of Bath.
[‡] University of Bristol.
[§] Chemicrea Inc.

(1) Chiba, Y.; Islam, A.; Watanabe, Y.; Komiya, R.; Koide, N.; Han, L. Y. *Jpn. J. Appl. Phys., Part 2* **2006**, *45*, L638−L640.
(2) Nazeeruddin, M. K.; Zakeeruddin, S. M.; HumphryBaker, R.; Jirousek, M.; Liska, P.; Vlachopoulos, N.; Shklover, V.; Fischer, C. H.; Gratzel, M. *Inorg. Chem.* **1999**, *38*, 6298−6305.
(3) Nazeeruddin, M. K.; Pechy, P.; Renouard, T.; Zakeeruddin, S. M.; Humphry-Baker, R.; Comte, P.; Liska, P.; Cevey, L.; Costa, E.; Shklover, V.; Spiccia, L.; Deacon, G. B.; Bignozzi, C. A.; Graetzel, M. *J. Am. Chem. Soc.* **2001**, *123*, 1613−1624.
(4) Bach, U.; Lupo, D.; Comte, P.; Moser, J. E.; Weissortel, F.; Salbeck, J.; Spreitzer, H.; Gratzel, M. *Nature* **1998**, *395*, 583−585.
(5) Kruger, J.; Plass, R.; Cevey, L.; Piccirelli, M.; Gratzel, M.; Bach, U. *Appl. Phys. Lett.* **2001**, *79*, 2085−2087.
(6) Kruger, J.; Plass, R.; Gratzel, M.; Cameron, P. J.; Peter, L. M. *J. Phys. Chem. B* **2003**, *107*, 7536−7539.
(7) Garcia-Canadas, J.; Fabregat-Santiago, F.; Bolink, H. J.; Palomares, E.; Garcia-Belmonte, G.; Bisquert, J. *Synth. Met.* **2006**, *156*, 944−948.
(8) Kay, A.; Humphrybaker, R.; Gratzel, M. *J. Phys. Chem.* **1994**, *98*, 952−959.

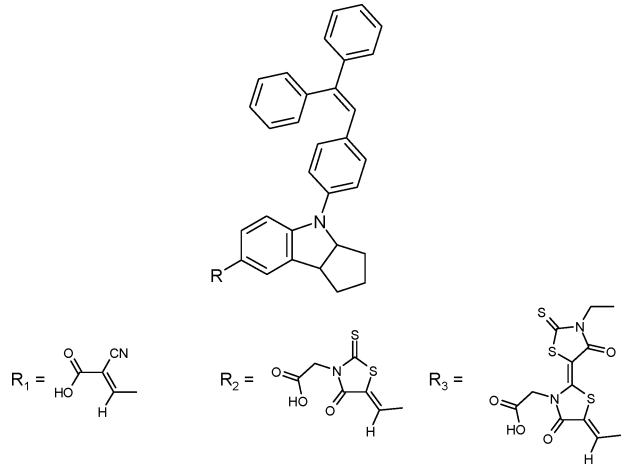

Figure 1. Molecular structures of the indoline dyes D102 (R_2), D131 (R_1), and D149 (R_3).

are used to minimize loss in current densities due to series resistance.[9] High molar extinction coefficient dyes are therefore desirable in order to make thin cells with good light-harvesting, and solid-state cells using an indoline dye and based on spiro-MeOTAD or CuI have achieved efficiencies of over 4%.[9,10] Here we present a detailed study of the properties of spiro-MeOTAD DSCs fabricated using nanocrystalline TiO_2 films sensitized with three recently developed high molar extinction coefficient metal-free indoline dyes.[11−13] The dyes investigated are referred to as D102, D131, and D149 (structural formulas shown in Figure 1), and their molar extinction coefficients (D102, $\epsilon = 58{,}800$ M^{-1} cm^{-1} at 491 nm; D131, $\epsilon = 48{,}000$ M^{-1} cm^{-1} at 425 nm; D149 $\epsilon = 68{,}700$ M^{-1} cm^{-1} at 526 nm) are significantly higher than those for the Ru dyes used in conventional electrolyte cells. As a consequence, complete light absorption at the peak wavelength can be achieved for films as thin as 1.6 μm.[9] The indoline dyes contain an arylamine moiety that acts as an electron donor and that is joined to a carboxylic moiety that functions as an electron acceptor and also as an anchoring group to attach the dye to the nanocrystalline TiO_2. When these dyes are absorbed on TiO_2 films, their absorption maxima are substantially red-shifted compared with the values in solution, making them favorable for light harvesting (see Supporting Information). Since these dyes can be synthesized and purified cheaply, an evaluation of their performance is of considerable interest in the context of future commercial exploitation of solid-state DSCs. The purpose of the present work was to achieve deeper insight into the factors that determine the performance of solid-state DSCs utilizing this type of dye.

Provided that electron injection is efficient (good overlap of the dye LUMO level with the conduction band of the oxide), the high extinction coefficient of the indoline dyes is expected to improve short circuit currents. However, the cell efficiency also depends on the open circuit voltage V_{oc}, which is determined by the energy difference between the quasi-Fermi level (QFL) of electrons in the nanocrystalline oxide under illumination and the redox level of the HTM. The QFL is controlled by the balance between electron injection and back reaction of the electrons with the HTM and the oxidized dye. This balance is affected by three principal factors: light harvesting/injection efficiency, shifts in the position of the TiO_2 conduction band relative to the redox level, and retardation (blocking) of back transfer of electrons to the HTM.[14] In order to deconvolute these effects as far as possible, we have investigated the photovoltage response, electron lifetimes, and electron trap distributions of spiro-MeoTAD-based DSCs using D102, D131, and D149 sensitizers and have correlated these properties with device performance.

Control of the conduction band energy is essential for DSC optimization, and one can speculate that tuning of the band energy might be achieved by choosing dyes with appropriate dipole moments. For this reason, density functional theory (DFT) calculations were used to determine the dipole moments of the three dye molecules in order to predict their contributions to the surface dipole, χ_{dip}, at the TiO_2/spiro-MeOTAD interface as a function of orientation and coverage. The predicted changes in χ_{dip} were compared with experimental observations of the shifts in conduction band energy deduced from the voltage dependence of the trapped electron density.[15,16]

Experimental Section

Device Preparation. DSCs were fabricated on fluorine-doped tin oxide glass (Tec 15, Libbey Owens Ford, sheet resistance 15 Ω cm) coated with a compact layer of TiO_2 prepared by spray pyrolysis of a solution consisting of 0.2 M titanium di-isopropoxide bis(acetylacetonate) (97%, Aldrich) in propan-2-ol.[18] Nanocrystalline TiO_2 films (Solaronix HT, particle size 9 nm, BET specific area 165 m^2/g) were spread on the compact layers by doctor-blading and annealed in air for 1 h at 450 °C to give thicknesses of 1.6−3.0 μm (measured by profilometry). The films were cooled to room temperature and immersed overnight in 0.02 M aqueous $TiCl_4$.[17] The films were then rinsed with deionized water and annealed in air at 450 °C for 20 min, after which they were cooled to 90 °C and sensitized by immersion in the appropriate dye solution for 12 h at room temperature. The dye solutions used were 0.5 mM D102, D131, or D149 dissolved in 50:50 vol % acetonitrile/*tert*-butanol. The solution for spin coating the hole-transport medium consisted of 0.18 M spiro-MeOTAD (Avecia), 0.11 M *tert*-butyl pyridine, 0.21 mM $Li[(CF_3SO_2)_2N]$, and 0.26 mM $N(p\text{-}C_6H_4Br)_3SbCl_6$ in chlorobenzene. A gold electrode was evaporated through a shadow mask onto the hole-transport material to complete the cell.

Device Characterization. Incident photon current efficiency (IPCE) spectra were measured using illumination from a 150 W Xe lamp/grating monochromator calibrated with a silicon photodiode (traceable ± 5% to NBS). Photovoltage decay measurements were performed under open circuit conditions using an Autolab PGSTAT 12 and a high-intensity green light-emitting diode (LED; $\lambda = 530$ nm). The cell was illuminated until a photostationary state was obtained, after which the LED was switched off and the photovoltage transient was recorded. Charge extraction measurements were performed using an instrument described previously[16] and recorded using a digital oscilloscope. In the charge extraction experiment, the cell is illuminated at open circuit

(9) Schmidt-Mende, L.; Gratzel, M. *Thin Solid Films* **2006**, *500*, 296−301.
(10) Konno, A.; Kumara, G. R. A.; Kaneko, S.; Onwona-Agyeman, B.; Tennakone, K. *Chem. Lett.* **2007**, *36*, 716−717.
(11) Horiuchi, T.; Miura, H.; Uchida, S. *Chem. Commun.* **2003**, 3036−3037.
(12) Horiuchi, T.; Miura, H.; Uchida, S. *J. Photochem. Photobiol., A* **2004**, *164*, 29−32.
(13) Ito, S.; Zakeeruddin, S. M.; Humphry-Baker, R.; Liska, P.; Charvet, R.; Comte, P.; Nazeeruddin, M. K.; Pechy, P.; Takata, M.; Miura, H.; Uchida, S.; Gratzel, M. *Adv. Mater.* 2006, *18*, 1202.
(14) Neale, N. R.; Kopidakis, N.; van de Lagemaat, J.; Gratzel, M.; Frank, A. J. *J. Phys. Chem. B* **2005**, *109*, 23183−23189.
(15) Bailes, M.; Cameron, P. J.; Lobato, K.; Peter, L. M. *J. Phys. Chem. B* **2005**, *109*, 15429−15435.
(16) O'Regan, B. C.; Durrant, J. R. *J. Phys. Chem. B* **2006**, *110*, 8544−8547.
(17) Sommeling, P. M.; O'Regan, B. C.; Haswell, R. R.; Smit, H. J. P.; Bakker, N. J.; Smits, J. J. T.; Kroon, J. M.; van Roosmalen, J. A. M. *J. Phys. Chem. B* **2006**, *110*, 19191−19197.
(18) Cameron, P. J.; Peter, L. M.; Hore, S. *J. Phys. Chem. B* **2005**, *109*, 930−936.

with a high-intensity green LED ($\lambda = 530$ nm) until a photostationary state is reached. Illumination is then interrupted, and the photovoltage is recorded for specified period before the cell is short circuited through a small measuring resistor via a fast relay switch. The observed current due to extraction of the remaining electrons in the nanocrystalline film is recorded as a current transient, which is integrated using a low-drift chopper-stabilized integrator to give the trapped charge. In a series of measurements, the amount of trapped charge was measured as a function of photovoltage by varying the delay before short circuiting the cells. The extracted charge was corrected for interfacial charging of the substrate using the measured capacitance of the blocking layer,[15,18,19] and the corresponding trapped electron density was calculated using the thickness of the film measured by profilometry. No correction was made for porosity.

The current−voltage characteristics of the cells were measured using a xenon arc solar simulator (ELLSOL 1000, model SVX 1450) with an AM 1.5 spectral filter, and the intensity was adjusted to provide 1 sun (100 mW cm^{-2}) using a calibrated GaAs solar cell.

Intensity-modulated photovoltage spectroscopy (IMVS) measurements used a Solartron 1250 frequency response analyzer to drive a high-intensity green LED ($\lambda = 530$ nm) and to analyze the frequency-dependent photovoltage response of the cells. The LED supplied the ac (modulation depth 10%) and dc components of the illumination. Photovoltages were measured as a function of intensity over a range of light intensities up to 12 mWcm^{-2} using a high-intensity green LED ($\lambda = 530$ nm) and a high impedance low-noise preamplifier (Stanford SR560). The light intensity was adjusted using neutral density filters (Schott NG) and measured using a calibrated silicon photodiode.

In order to determine dye loadings, sensitized electrodes were immersed in 0.36 M KOH in methanol to desorb the dyes, and the amount of the dye was calculated from the UV/visible absorbance. The stability of the desorbed dye in the alkaline solution was established by UV/vis spectroscopy in a separate series of experiments.

Computational Details

The structures of both the protonated and deprotonated forms of the D102, D131, and D149 dyes were optimized at the B3LYP level of theory using a 6-31G* basis set with the Jaguar program (Jaguar, 6.0, Schrödinger, Inc., Portland, Oregon). It is known that molecules containing a carboxylate group bind chemically to the nanocrystalline TiO_2 surface.[20,21] Since the dye molecules are chemisorbed onto the TiO_2 surface, the protonated forms of the dye were considered in the calculations of the dipole moment, although the dipole moments were also calculated for the deprotonated forms for comparison. Possible isomers of the organic dyes were calculated by initially setting the double bond torsional values to either *cis* or *trans* geometry. Additionally, potential rotamers of D102 and D149 were studied by rotating the torsional angle centered along the N−C bond linking the carboxylate group to the rest of the molecule (see Supporting Information). This doubles the number of possible conformations of D102 and D149, but it was found that neither the energy nor the dipole moment (and its direction) of corresponding rotamers changes significantly upon torsion. To investigate solvent effects, the calculations were carried out using the self-consistent reaction field (SCRF) method[22] for both acetonitrile (dielectric constant $\epsilon = 35.69$, probe radius = 2.18 Å) and *tert*-butanol (dielectric constant $\epsilon = 12.47$, probe radius = 2.66 Å). The energy order of the conformers was found to be unaffected by the choice of solvent. Since D102, D131, and D149 dyes are synthesized in a polar solvent (acetic acid[10]), it was assumed that under thermodynamic control only the low-energy structures are produced. Consequently, only the lowest-energy solvated structures (within 3 kcal/mol of the minimum energy structure) were considered in the calculations.

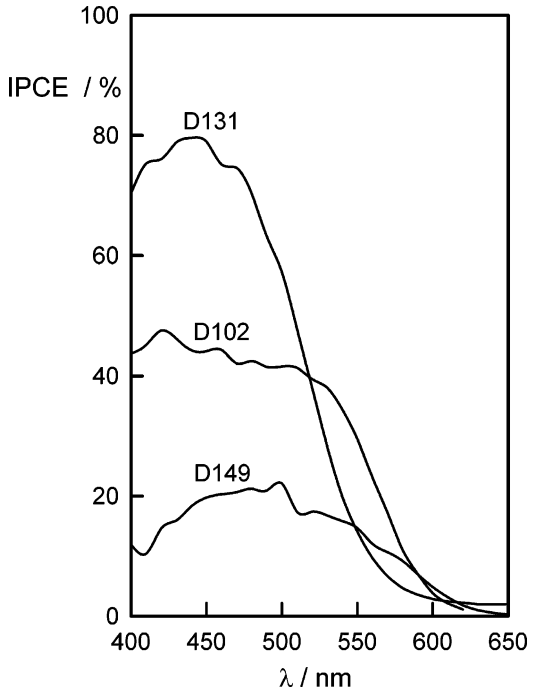

Figure 2. IPCE spectra of spiro-MeOTAD cells sensitized with the three indoline dyes. TiO_2 film thickness: D102, 2.4 μm; D131, 3.0 μm; D149, 1.6 μm. Since all three cells absorb the entire incident light at the peak absorption wavelength, the variation in peak IPCE directly reflects the different injection efficiencies of the dyes.

Results and Discussion

IPCE Spectra. The IPCE (external quantum efficiency) of a DSC is determined by the product of the light harvesting, electron injection, and electron collection efficiencies. Figure 2 compares the IPCE spectra of spiro-MeOTAD DSCs sensitized with D102, D131, and D149. For D102 and D149, the IPCE spectra are consistent with the reported absorption spectra of the dyes adsorbed on nanocrystalline TiO_2 films[11,23] (see Supporting Information for the absorption spectrum of adsorbed D131 dye). The IPCE value for the D102 cell is similar to that reported by Schmidt-Mende et al.[24]

For the same dye loading and TiO_2 film thickness, one might expect the peak IPCE values to follow the trend in extinction coefficients, D149 > D102 > D131. However, Figure 2 shows that the order of the IPCE values is in fact *reversed*. This could in principle be due to differing dye coverage, quenching of the excited-state due to dye aggregation, or differing degrees of overlap of the LUMO level of the dyes with the TiO_2 conduction band. The loading of all three dyes was determined by dye desorption, and in all cases the absorbance of the films was

(19) Cameron, P. J.; Peter, L. M. *J. Phys. Chem. B* **2005**, *109*, 7392−7398.
(20) Nazeeruddin, M. K.; Bessho, T.; Cevey, L.; Ito, S.; Klein, C.; De Angelis, F.; Fantacci, S.; Comte, P.; Liska, P.; Imai, H.; Graetzel, M. *J. Photochem. Photobiol., A* **2007**, *185*, 331−337.
(21) Meyer, T. J.; Meyer, G. J.; Pfennig, B. W.; Schoonover, J. R.; Timpson, C. J.; Wall, J. F.; Kobusch, C.; Chen, X. H.; Peek, B. M.; Wall, C. G.; Ou, W.; Erickson, B. W.; Bignozzi, C. A. *Inorg. Chem.* **1994**, *33*, 3952−3964.
(22) Tapia, O.; Goscinski, O. *Mol. Phys.* **1975**, *29*, 1653−1661.
(23) Horiuchi, T.; Miura, H.; Sumioka, K.; Uchida, S. *J. Am. Chem. Soc.* **2004**, *126*, 12218−12219.
(24) Schmidt-Mende, L.; Bach, U.; Humphry-Baker, R.; Horiuchi, T.; Miura, H.; Ito, S.; Uchida, S.; Gratzel, M. *Adv. Mater.* 2005, *17*, 813.

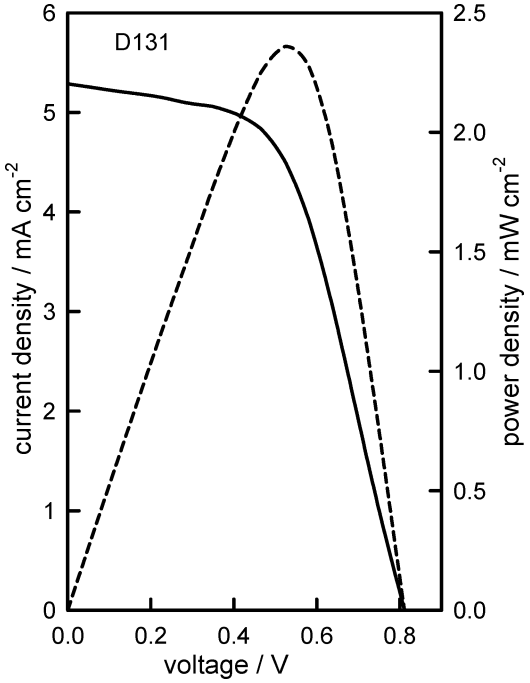

Figure 3. AM 1.5 *IV* characteristic of a spiro-MeoTAD cell sensitized with D131. TiO_2 film thickness, 3.0 μm. The power characteristic is shown as a broken line.

Table 1. Performance of Spiro-MeOTAD Cells Sensitized with D102, D131, and D149

dye	I_{sc} (mA cm^{-2})	IPCE (%)	predicted I_{sc} (mA cm^{-2})	V_{oc} (mV)	FF	η (AM1.5)	coverage (cm^{-2})	η_{inj} (%)
D102	4.6	42	4.2	855	0.70	2.8	3.6×10^{13}	42
D131	5.3	77	5.6	809	0.56	2.4	6.3×10^{13}	77
D149	2.3	16	2.0	872	0.75	1.5	3.6×10^{13}	16

sufficiently high that the incident light should be completely absorbed at the wavelength corresponding to the maximum absorption coefficient. It follows from this that the peak IPCEs for the different dyes are essentially equivalent to the injection efficiencies. The values are: D102, 42%; D131, 77%; D149, 16%.

Since light absorption is complete, the differing IPCE values indicate that the sensitizer injection efficiencies in spiro-MeOTAD based cells vary in the order D149 < D102 < D131. By contrast, the reported IPCE values for of liquid electrolyte-based DSCs sensitized by D102 and D131 are both in the range 75−85%, which suggests that the injection efficiencies are higher in these systems.[24] The lower electron injection efficiencies in the solid-state system could be due to poor overlap of the dye LUMO level with the conduction band of the TiO_2 or from back reaction with the oxidized dye.

I−V Characteristics. The I−V characteristics of the cells were measured under AM 1.5 1 sun illumination. As an example, Figure 3 illustrates the I−V characteristics for a D131-sensitized cell. The short circuit current densities for all of the cells under solar illumination were predicted by convolution of the IPCE spectra with the photon flux density distribution for 1 sun (AM 1.5). The values obtained from the IPCE spectra in Figure 2 are listed in Table 1 together with the open circuit voltages, fill factor, solar efficiencies, measured dye coverages, and injection efficiencies. The experimental short circuit current values agree well with those predicted from the IPCE, indicating that the cells exhibit a linear current response up to 1 sun.

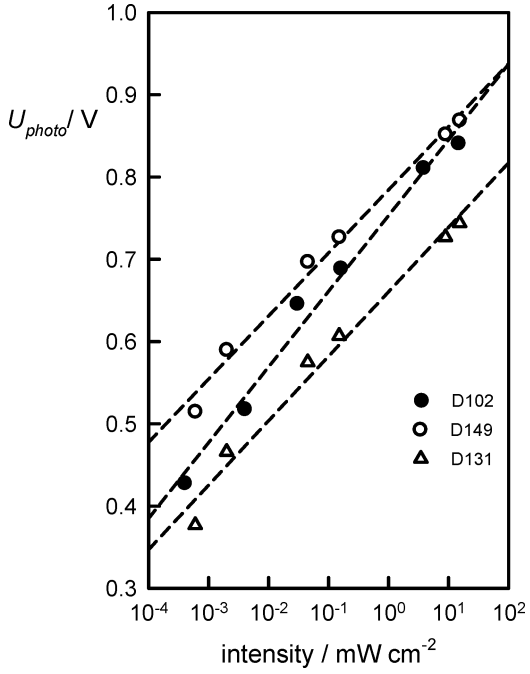

Figure 4. Intensity dependence of photovoltage for spiro-MeOTAD cells sensitized with D102, D131, and D149.

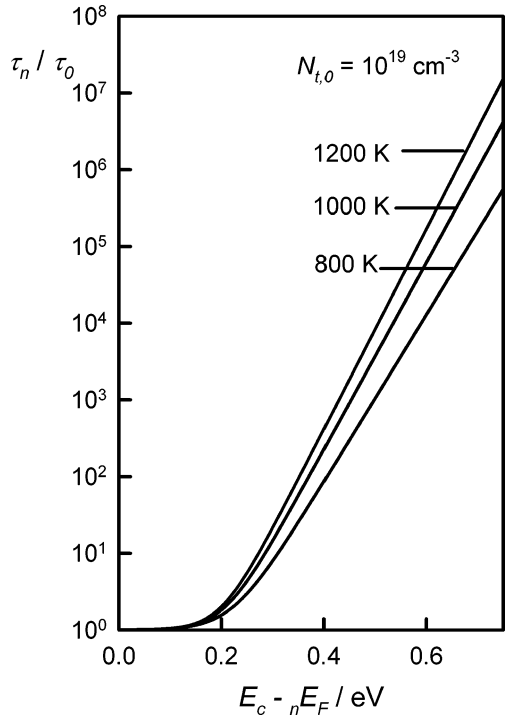

Figure 5. Variation of normalized electron lifetime τ_n/τ_0 calculated using the quasi-static approach as a function of the position of the electron QFL relative to the conduction band. $N_{t,0}$ and T_0 as shown.

Intensity Dependence of V_{oc}. The semilogarithmic plots in Figure 4 compare the intensity dependence of V_{oc} for three spiro-MeOTAD cells sensitized with D102, D131, and D149. The results indicate that for all three cells, V_{oc} depends linearly on the logarithm of light intensity. The slopes of the plots are 64 mV/decade for the D102-sensitized cell and 79 mV/decade for both the D131-sensitized cell and the D149-sensitized cell. The slopes are similar to those observed for iodide/tri-iodide electrolyte DSCs (with blocking layers) fabricated with the same

TiO_2 colloid and sensitized with N719, which lie in the range from 70 to 80 mV/decade. Since the plots are linear down to low light intensities (<2 μW cm^{-2}), it is evident that back reaction via the substrate is negligible as a consequence of the diode properties of the compact TiO_2 blocking layer.[19] Recombination of electrons with holes in the spiro-MeOTAD therefore occurs predominantly via the nanocrystalline TiO_2. The plots in Figure 4 also show that the V_{oc} of the D149 cells is 120 mV higher than the V_{oc} of the D131 cell, in spite of the fact that the IPCE of the D131 cell at 530 nm is twice that of the D149 cell, indicating a higher rate of electron injection. It follows that the higher V_{oc} of the D149 cell is not a consequence of more efficient light harvesting. Instead it points either to a reduction in the rate constant for the back reaction of electrons with holes or to an upward movement of the TiO_2 conduction band energy relative to the spiro-MeOTAD redox level.[13,25]

Measurements of Electron Lifetime. The apparent electron lifetimes for the three cells were measured as a function of photovoltage using IMVS and the photovoltage decay technique. According to the quasi-static treatment developed by Bisquert and Vikhrenko,[26] the apparent electron lifetime, τ_n, is related to the conduction band electron lifetime, τ_0, by the expression

$$\tau_n = \tau_0\left(1 + \frac{\partial n_t}{\partial n_c}\right) \quad (1)$$

where n_t is the trapped electron density, n_c is the conduction band electron density, and τ_0 is the inverse of the pseudo-first-order rate constant for the back transfer of electrons from the conduction band (it should be noted that the derivation of eq 1 assumes that electrons are transferred to the HTM only via the conduction band and not via surface states). The intensity dependence of τ_n arises from the fact that n_t and n_c depend on the photovoltage in different ways. The commonly encountered exponential distribution of electron traps in the nanocrystalline TiO_2 is described by the expression

$$g(E_T) = \frac{N_{t,0}}{k_B T_0}\exp\left[-\frac{(E_c - E_T)}{k_B T_0}\right] \quad (2)$$

Here $E_c - E_T$ is the trap depth below the conduction band, $N_{t,0}$ is the total trap density and $k_B T_0$ is a characteristic energy describing the width of the distribution. It can be shown that the variation of the apparent electron lifetime with photovoltage in the case of an exponential distribution of electron traps is given by

$$\log_{10}\tau_n = \text{constant} + (\beta - 1)\frac{qU_{photo}}{2.303 k_B T} \quad (3)$$

where $\beta = T/T_0$ can be determined from the slope of a semilogarithmic plot of log τ_n vs photovoltage.

Figure 5shows how the ratio τ_n/τ_0 (calculated from eqs 1 and 2) varies as the electron QFL is changed by altering the illumination level. The calculation was performed for three values of T_0 that are comparable with those observed experimentally. This plot allows the value of τ_0 to be estimated if T_0 and $N_{t,0}$ are known. The estimation of τ_0 also requires knowledge

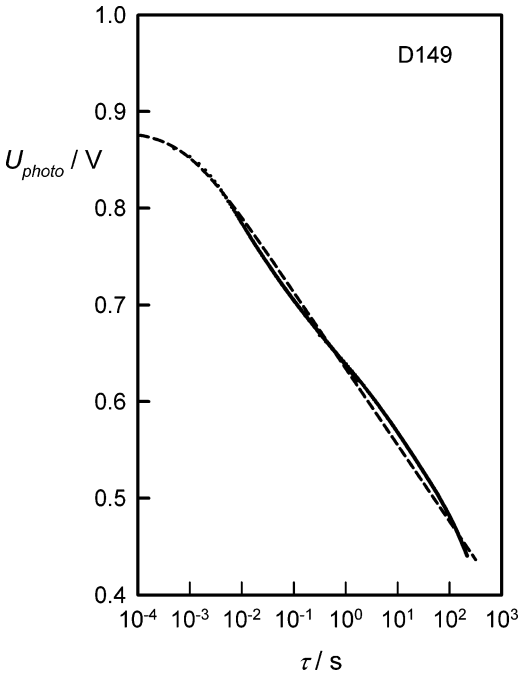

Figure 6. Open circuit photovoltage decay for spiro-MeOTAD cell sensitized with D149. The fit to eq 5 is shown as a broken line.

do the energy difference between E_c, the conduction band energy, and $E_{F,redox}$, the Fermi energy of the contacting phase.

τ_n for cells fabricated with the three indoline dyes was determined as a function of photovoltage by IMVS as well as by analysis of the photovoltage decay transients following the approach of Zaban[27] and Bisquert:[28]

$$\tau_n = -\frac{k_B T}{q}\left(\frac{dU_{photo}}{dt}\right)^{-1} \quad (4)$$

Figure 6 shows the photovoltage decay in semilogarithmic form for the D149 cell. The decay fits well to the form expected for an exponential distribution of traps, which is given by[29]

$$U_{ph,qs} = -\frac{k_B T}{q(1 - T/T_0)}(\ln|c_2| + \ln(t)) \quad (5)$$

where

$$c_1 = \exp\left[\frac{(T/T_0 - 1)qU_{ph}(0)}{k_B T}\right] \text{ and } c_2 = k_{cb}\left[1 - \frac{T}{T_0}\right]\frac{N_C T_0}{N_{t,0} T}\left(\frac{n_{eq}}{N_C}\right)^{(1 - T/Tc)} \quad (6)$$

The slope of the semilogarithmic decay plot at long times is given by

$$\frac{dU_{photo}(t)}{d\ln t} = -\frac{k_B T}{q\left(1 - \frac{T}{T_0}\right)} \quad (7)$$

The fit gives $\beta = T/T_0 = 0.27$, $T_0 = 1100$ K.

(25) Hara, K.; Horiguchi, T.; Kinoshita, T.; Sayama, K.; Sugihara, H.; Arakawa, H. *Sol. Energy Mater. Sol. Cells* **2000**, *64*, 115−134.
(26) Bisquert, J.; Vikhrenko, V. S. *J. Phys. Chem. B* **2004**, *108*, 2313−2322.
(27) Bisquert, J.; Zaban, A.; Greenshtein, M.; Mora-Sero, I. *J. Am. Chem. Soc.* **2004**, *126*, 13550−13569.
(28) Zaban, A.; Greenshtein, M.; Bisquert, J. *ChemPhysChem* **2003**, *4*, 859−864.
(29) Walker, A. B.; Peter, L. M.; Lobato, K.; Cameron, P. J. *J. Phys. Chem. B* **2006**, *110*, 25504−25507.

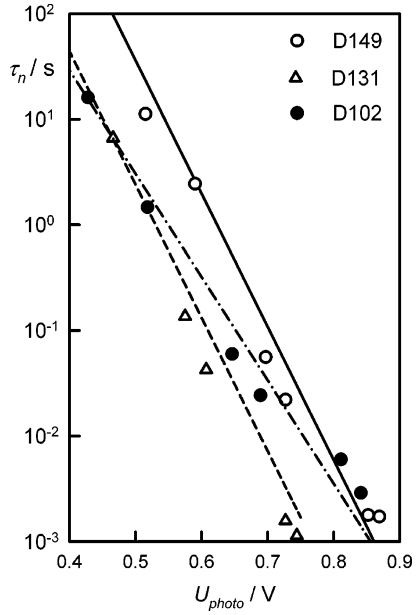

Figure 7. Electron lifetimes derived for spiro-MeoTAD cells sensitized with D102, D131, and D149. The plot compares data obtained from fitting of photovoltage decay curves (lines) compared with values measured by intensity modulated photovoltage spectroscopy (points).

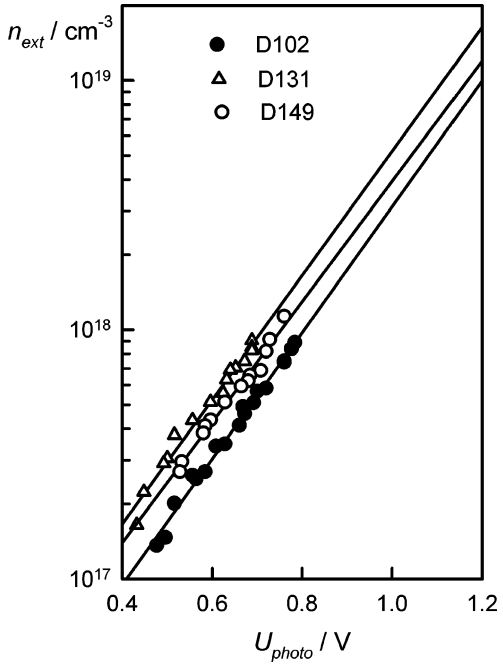

Figure 8. Trapped electronic charge as a function of photovoltage measured by the charge extraction technique for spiro-MeOTAD cells sensitized with D102, D131, and D149. The parallel displacement of the plots along the photovoltage axis shows that the TiO_2 conduction band energy relative to the spiro-MeOTAD redox level increases in the order D131 < D149 < D102.

Fits to eqs 4 and 5 were used to derive the dependence of τ_n on photovoltage from the photovoltage decay for the three cells. Figure 7 compares the semilogarithmic lifetime plots obtained in this way with the τ_n values determined by IMVS with different levels of steady-state illumination. The good agreement confirms the validity of the approach. The $\beta = T/T_0$ values obtained from this photovoltage decay analysis are: $\beta = 0.41$, $T_0 = 720$ K for D102-sensitized devices; $\beta = 0.27$, $T_0 = 1100$ K for D149-sensitized devices, and $\beta = 0.27$, $T_0 = 1100$ for D131-sensitized devices.

Determination of Relative Positions of the TiO_2 Conduction Band. Since the TiO_2 colloid used in all three cells is the same, the trap distribution involved in electron transport should be identical, and one would therefore expect the slopes of the semilogarithmic plots of τ_n vs photovoltage to be the same for all three dyes. The slopes are indeed the same for the D149 and D131 cells, but the D102 cell gives a different slope in the semilogarithmic plots of τ_n vs U_{photo} as well as in the U_{photo} vs intensity plot.

The data in Figure 7 show that for the D149 cell, τ_n at a given photovoltage is more than an order of magnitude larger than τ_n for the D131 cell. This is consistent with the fact that higher photovoltages are obtained with the D149 cell, in spite of the fact that it has the lowest IPCE. Possible causes of this difference are an upward shift of the TiO_2 conduction band in the presence of D149 or a lowering by D149 of the rate of electron transfer to the HTM as a consequence of partial blocking of electron transfer. The first explanation is more likely, since an upward shift of the conduction band would also rationalize the low IPCE of the D149 cells if it is sufficient to produce a mismatch with the LUMO level of the dye.

To determine whether the differences in photovoltage for the D102, D149, and D131 cells are simply due to shifts in their conduction band energies, the density and distribution of electron traps was investigated for the three cells using the charge extraction method.[16] The density of states function for an exponential distribution of electron traps is given by eq 2, which can be rewritten in a form that shows explicitly the dependence of $g(E)$ on photovoltage:

$$g(_nE_F) = \left[\frac{N_{t,0}}{k_B T_0} \exp - \left(\frac{E_c - E_{F,redox}}{k_B T_0}\right)\right] \exp\left(\frac{qU_{photo}}{k_B T_0}\right) \quad (8)$$

For a film of thickness d, the number of electrons extracted when the cell is short circuited at a photovoltage of U_{photo} is given in the zero K approximation and for $qU_{\text{photo}}/k_BT_0) > 1$ by

$$n_{ext} = d \int_{E_{F,redox}}^{E_{F,redox} + qU_{photo}} f_{FD}(E) g(e) dE \cong N_{t,0} \exp - \left(\frac{E_c - E_{F,redox}}{k_B T_0}\right) \exp \frac{qU_{photo}}{k_B T_0} \quad (9)$$

so that a plot of log n_{ext} vs U_{photo} has a slope of $(2.303k_BT_0)^{-1}$ and an intercept of $N_{t,0}$ exp $-(E_c - E_{F,redox}/2.303k_BT_0)$. Figure 8 shows semilogarithmic plots of the extracted electron densities (corrected for substrate charging) as a function of photovoltage for cells sensitized by the three dyes. The linear regression fits (shown as lines) confirm that the traps have an exponential energy distribution. Since the trap distribution is a bulk property of the TiO_2 nanoparticles, the relative displacement of the plots on the photovoltage axis indicates that the conduction band energy is not the same for cells fabricated with the three dyes. The results show that conduction band energy follows the sequence D102 > D149 > D131, with that of D131 100 meV higher than that of D102. This conclusion is consistent with the electron lifetime plots in Figure 6, which show similar displacements.

Analysis of the charge extraction data for D102, D149, and D131 dyes gives $T_0 = 2100$ K ($\beta = 0.14$). The β value obtained

from the charge extraction plots is considerably lower than the values derived from the semilogarithmic lifetime plots. This is also the case for electrolyte cells, and the discrepancy can be traced back to the fact that the derivation of eq 3 assumes that electron transfer to the HTM takes place only from the conduction band. If this were the case, the photovoltage vs log(intensity) plots would have slopes of 59 mV/decade at 300 K. In practice, the slopes are 65−79 mV/decade (cf. Figure 4). This non-ideality probably indicates that electron transfer also occurs via surface states.[30] Interestingly, the deviation from ideality in both photovoltage and lifetime plots is largest for the D102 cell, and this may indicate that dye adsorption introduces additional surface states at the TiO_2 surface. A quantitative treatment of electron transfer via surface states is precluded by the absence of information about their density and energetic distribution. However, attempts to optimize dye-sensitized solar cells should consider the elimination of surface states as a route for the back transfer of electrons.

Shifts in the TiO_2 conduction band energy arise from changes in the surface dipole potential[31,32] at the TiO_2|HTM interface. Unfortunately, DSCs are complex systems, with competing adsorption by dye molecules, solvent, additives (*tert*-butyl pyridine), electrolyte ions and protons released by the carboxylate groups on the dyes during adsorption. Nevertheless, an interesting question is whether the dye monolayer plays an important role in controlling the surface dipole potential, so that the conduction band energy could be tuned by choosing dyes with different dipole moments. This question was investigated by calculating the dipole moments of the dyes, and hence their contribution to the surface dipole potential as a function of orientation and surface coverage.

Normalization of the Lifetime Plots To Obtain τ_0 Values. In order to compare the relative rates of transfer of electrons to the oxidized form of spiro-MeOTAD in cells fabricated with the three indoline dyes, it is necessary to eliminate the effects due to different conduction band energies. This can be done using the information obtained from the charge extraction experiments (cf. Figure 7). The first step in the calculation involves finding a self-consistent value of $E_c - E_{F,redox}$ for the D131 cell. The value of $E_c - E_{F,redox}$ determines τ_0 and hence the steady-state conduction band electron density, which is given by

$$n_c = \frac{I_0 \Phi \tau_0}{d} = N_c \exp - \left(\frac{E_c - {}_nE_F}{k_B T} \right) = N_c \exp - \left(\frac{E_c - E_{F,redox} + qU_{photo}}{k_B T} \right) \quad (10)$$

Here I_0 is the incident photon flux, Φ is the IPCE, and d is the film thickness. The value of $E_c - E_{F,redox}$ also determines the value of the total trap density, $N_{t,0}$, derived from the plot in Figure 8. $N_{t,0}$ and T_0 are required to calculate the ratio τ_n/τ_0 (cf. Figure 5). $T_0 = 1100$ K is obtained from the slopes of the lifetime plot in Figure 7. The value of N_c was taken to be 10^{21} cm^{-3} for the self-consistent calculation of $E_c - E_{F,redox}$ for the D131 cell. This procedure gave $N_{t,0} = 10^{19}$ cm^{-3}, $E_c - E_{F,redox} = 1.10$ eV and $\tau_0 = 10^{-5}$ s. Using the shifts of the charge extraction plots seen in Figure 8, it can be concluded that the values of $E_c - E_{F,redox}$ for the D102 and D149 cells are 1.200 and 1.135 eV, respectively. Figure 9 shows the lifetime data replotted as function of $E_c - E_{F,redox}$. The fit to the data for the D131 cell shown in Figure 9 gives a conduction band electron lifetime of 1.5×10^{-5} s. The best-fit values for the D102 and D149 cells are 10^{-4} s and 1.5×10^{-4} s, respectively. In the case of the D 102 cell, the value of T_0 was changed from 1100 to 700 K to obtain a fit.

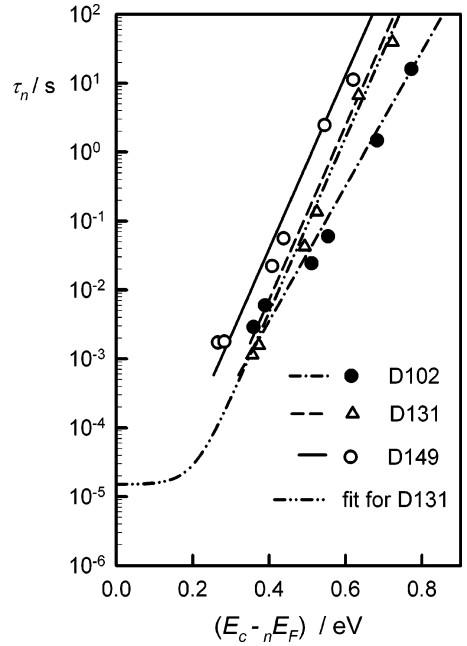

Figure 9. Plots of apparent electron lifetimes as a function of $E_c - E_{F,redox}$. The points correspond to data obtained by IMVS, the lines to fits of the photovoltage decays. The fitting of the data to the quasi-static model is illustrated for the D131 cell. The intercept give $\tau_0 = 1.5 \times 10^{-5}$ s. Values used in the fit: $N_c = 10^{21}$ cm^{-3}, $N_{t,0} = 10^{19}$ cm^{-3}, $T_0 = 1100$ K.

DFT Calculations. The lowest energy molecular orbitals (LUMO) for the protonated dyes (D102, D131, and D149) in acetonitrile were derived from the DFT calculations. The physical separation of the electron-donating (ED) and electron-accepting groups (EA) for D131, D102, and D149 dyes are 8.13, 10.90, and 10.86 Å, respectively. In all cases studied, the HOMO is delocalised over the π system with the highest electron density centered on the central nitrogen atom (see Supporting Information).

The LUMO is a π antibonding orbital localized toward the carboxylate moiety. The calculated HOMO−LUMO gaps are 2.51, 2.84, and 2.43 eV for the D102, D131, and D149 dyes, respectively, and this agrees well with the trends in absorption maxima of the dyes in solution[10,11] (see Supporting Information). The absolute energies of the HOMOs are −5.12, −5.21, and −5.06 eV, while the absolute energy of the LUMOs are −2.61, −2.37, and −2.63 eV for D102, D131, and D149, respectively. For comparison, the LUMO level for N719 (calculated at DFT level of theory in a water environment) is −2.7 eV with the HOMO at −5.3 eV.[21] The HOMO (conduction band) energy level of TiO_2 calculated for a $Ti_{38}O_{76}$ cluster exposing the

(30) Bisquert, J.; Zaban, A.; Salvador, P. *J. Phys. Chem. B* **2002**, *106*, 8774−8782.
(31) Ruhle, S.; Greenshtein, M.; Chen, S. G.; Merson, A.; Pizem, H.; Sukenik, C. S.; Cahen, D.; Zaban, A. *J. Phys. Chem. B* **2005**, *109*, 18907−18913.
(32) Kruger, J.; Bach, U.; Gratzel, M. *Adv. Mater. (Weinheim, Ger.)* **2000**, *12*, 447−451.

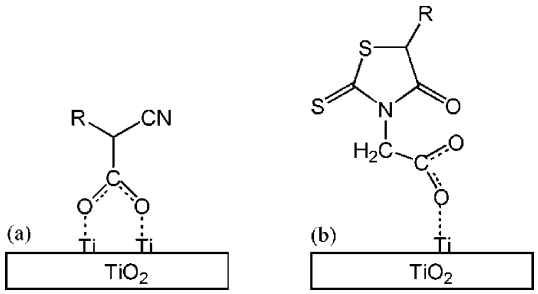

Figure 10. Bidenate and monodentate binding schemes for the indoline dyes.

anatase (101) surface[33] is located at −6.55 eV, and the corresponding LUMO, at −2.77 eV. Therefore, the DFT calculations suggest there is a reasonable alignment between the LUMO of all the dyes and the band edge of TiO_2 to facilitate charge injection,[34] although on the basis of the calculated values the injection efficiency might be expected to be lower for D131. However, it is important to point out that these comparisons of LUMO and conduction band energies neglect the surface dipole potentials. In fact the experimental evidence discussed above indicates that D149 gives the lowest injection efficiency due to an upward shift of the conduction band energy arising from the surface dipole potential.

The bidentate and monodentate bonding schemes for the attachment of the organic dyes to the TiO_2 surface are illustrated in Figure 10. If the bidentate bonding is preferred, D102 and D149 will lie along the surface of TiO_2 as shown in Figure 11, whereas D131 will stand up from the surface, giving more dense packing.

The Surface Dipole Potential. The monolayer coverages (estimated from the optimized molecular structures) for monodentate and bidentate bonding of dyes are given in Table 2, which compares them with the values measured by dye desorption. The maximum dye coverages were estimated for close packing from the optimized molecular structures obtained from DFT calculations. The experimental values were obtained by dye desorption. The orientation of the adsorbed dye molecules is shown in the table: ↑ standing up; → lying down. From this comparison, we conclude that all three dyes are adsorbed by bidentate binding, with D102 and D149 oriented parallel to the surface of TiO2 and D131 oriented vertically.

Table 3 lists the total dipole moments and the dipole moments normal to the surface corresponding to the monodendate and bidentate dye bonding scheme calculated in an acetonitrile environment for D102, D131, and D149 dyes. The dipole moment of the dyes points in the direction of the carboxylic acid group, i.e., the negative end is at the TiO_2|dye interface.

The normal surface dipole potential for a layer of dye molecules oriented at an angle θ from the normal is given by[32]

$$\chi_{dip} = \frac{N_{dip}\mu_{dip}\cos\theta}{\epsilon\epsilon_0} \qquad (11)$$

where N_{dip} is the coverage with dipoles, μ_{dip} is the molecular dipole moment, and ϵ_0 is the permittivity in a vacuum, and ϵ is

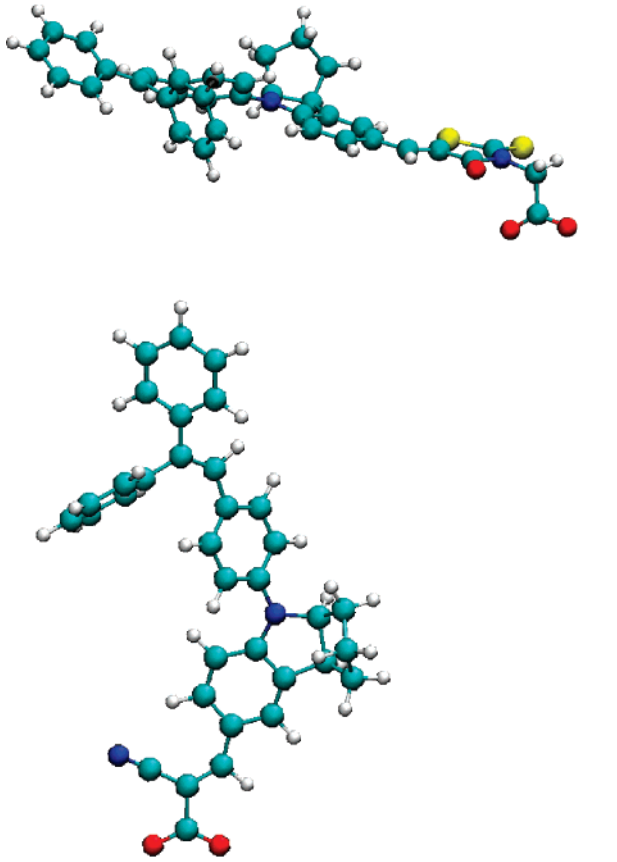

Figure 11. Predicted orientation of indoline dyes on TiO_2 for the case of bidentate binding. D102 (upper part of figure) and D149 (not shown) lie along the surface of TiO_2, whereas D131 (lower part of figure) stands up from the surface to give higher packing density.

Table 2. Calculated and Measured Dye Coverages for D102, D131, and D149

dye	modentate monolayer coverage (cm^{-2})	bidentate monolayer coverage (cm^{-2})	experimental coverage (cm^{-2})
D102	9.2×10^{13} ↑	4.0×10^{13} →	3.6×10^{13}
D131	–	1.7×10^{14} ↑	6.3×10^{13}
D149	6.6×10^{13} ↑	2.7×10^{13} →	3.6×10^{13}

Table 3. Calculated Dipole Moments for D102, D131, and D149

dye	total dipole (D)	normal component of dipole (D)	dipole potential (mV)
D102	11.2 ± 0.8	3.6 ± 0.5 →	92 ± 13
D131	12.0 ± 1.3	7.6 ± 0.9 ↑	340 ± 40
D149	12.0 ± 1.5	3.8 ± 1.0 →	97 ± 26

dielectric constant of the dipole layer. The dielectric constant for aromatic molecules in a monolayer is reported to be 5.3.[35,36] The surface dipole potentials listed in Table 3 were estimated from the calculated molecular dipole moments for bidentately bonded dyes using the dye coverage values measured by dye desorption (cf. Table 1).

According to these calculations, the upward shift in conduction band energy due to the surface dipole of the dyes should follow the order D102 ≈ D149 < D131 However, the charge

(33) De Angelis, F.; Tilocca, A.; Selloni, A. *J. Am. Chem. Soc.* **2004**, *126*, 15024−15025.
(34) Nazeeruddin, M. K.; De Angelis, F.; Fantacci, S.; Selloni, A.; Viscardi, G.; Liska, P.; Ito, S.; Takeru, B.; Gratzel, M. G. *J. Am. Chem. Soc.* **2005**, *127*, 16835−16847.
(35) Bruening, M.; Moons, E.; Yaronmarcovich, D.; Cahen, D.; Libman, J.; Shanzer, A. *J. Am. Chem. Soc.* **1994**, *116*, 2972−2977.
(36) Zuppiroli, L.; SiAhmed, L.; Kamaras, K.; Nuesch, F.; Bussac, M. N.; Ades, D.; Siove, A.; Moons, E.; Gratzel, M. *Eur. Phys. J. B* **1999**, *11*, 505−512.

extraction measurements indicate that the upward shift is in fact in the order D131 < D149 < D102. We conclude from this that the surface dipole potential caused by the absorption of the dye must be modified by other molecular and ionic species. Candidates are protons released during dye adsorption,[33,35] lithium ions present in the HTM, and the *tert*-butyl pyridine additive which shifts the conduction band energy upward in spiro-MeOTAD cells. It is likely that small cations such as protons or lithium ions will be able to penetrate the adsorbed dye layer (which does not behave as an ideal impermeable self-assembled monolayer) and adsorb at the TiO_2 interface, creating a surface dipole that moves the conduction band energy downward. The differences in surface charge required to cause the observed relative displacements of conduction band in D102, D149, and D131 cells are of the order of $3-4 \times 10^{12}$ cm^{-2}. We therefore conclude that the observed trends in conduction band energy revealed by the charge extraction experiments reflect the interplay of these opposing contributions to the surface dipole potential.

Conclusions

The measurements and calculations reported in this paper illustrate the utility of a coherent experimental and theoretical approach to the characterization of dye-sensitized solar cells. It is particularly important to measure the relative positions of the TiO_2 conduction band relative to the Fermi level of the hole-transport medium before attempting any comparison of electron lifetimes or drawing any conclusions about possible blocking of electron transfer. In the systems studied here, it is evident from the comparison of experimental data and theoretical predictions that there is a complex interplay of different factors that determine the position of the conduction band.

Acknowledgment. The work was supported by the EPSRC as part of the SUPERGEN Excitonic Solar cell Consortium programme (GR/T26559/01). F.C. thanks EPSRC for his Life Science Interface Fellowship.

Supporting Information Available: Absorption spectra of D102, D131, and D149 in solution and adsorbed on nanocrystalline TiO_2; HOMO and LUMO orbitals of D102, D131, and D149 obtained from DFT calculations; and torsional angles for D102, D131, and D149 used in DFT calculations. This material is available free of charge via the Internet at http://pubs.acs.org.

JA076525+